Do adsorbent screening metrics predict process performance? A process optimisation based study for post-combustion capture of CO$_2$

Ashwin Kumar Rajagopalan [1], Adolfo M. Avila [2], Arvind Rajendran*

Department of Chemical and Materials Engineering, University of Alberta, 12th Floor, 9211-116 Street NW Street, Edmonton, Alberta, Canada T6G 1H9

ABSTRACT

Recent interest in carbon dioxide capture has led to the development of hundreds of adsorbents. Adsorbent screening is typically performed either by inspecting the isotherms or by using simple adsorbent screening metrics (selectivities, working capacities, figures of merit, etc.). This work seeks to critically evaluate the efficacy of various adsorption metrics for adsorbent screening through the use of process-optimisation. A case study addressing post-combustion CO$_2$ capture using vacuum swing adsorption (VSA) is presented. Four different adsorbents (Mg-MOF-74, UTSA-16, Zeolite 13X and a type of activated carbon) were subjected to process-optimisation studies on a 4-step PSA cycle with light product pressurisation (LPP). Two kinds of process optimisation studies were performed. The first to maximise purity and recovery; and the second to minimise energy consumption and maximise productivity subject to purity/recovery constraints. This study highlights that most commonly used adsorbent metrics do not correctly rank adsorbents in order of their performance at a process scale. Further, it is also shown that N$_2$ affinity/capacity plays a critical role in deciding the process performance of VSA based post-combustion CO$_2$ capture.

1. Introduction

In the recent years, significant efforts have been invested in the synthesis of novel materials and processes to capture CO$_2$ from anthropogenic sources. Absorption, adsorption and membrane processes have been proposed over the years to capture CO$_2$ (Aaron and Tsouris, 2005; Xiao et al., 2008; Ebner and Ritter, 2009; Haghpanah et al., 2013b; Abanades et al., 2015). Within the category of adsorption processes pressure swing adsorption (PSA) and temperature swing adsorption (TSA) have been studied extensively. In designing an adsorption based separation process, the choice of adsorbent plays a crucial role (Ruthven, 1984; Yang, 1997). On the one hand, classical materials like Zeolite 13X, Activated Carbon have been studied extensively for CO$_2$ capture. On the other hand, novel materials like the metal organic frameworks (MOFs), Zeolitic imidazolate frameworks (ZIFs) have caught the attention due to the high CO$_2$ loading capacities and selectivity; some even in the presence of

moisture (Demessence et al., 2009; Britt et al., 2009; Zhang et al., 2014; Hu et al., 2015).

For any separation problem multiple adsorbents are initially considered and basic measurements, such as, single-component isotherms are measured. Once these measurements are available, adsorbent screening is traditionally performed based on the so-called "adsorbent metrics" that can be calculated using single-component isotherms. Many adsorbent metrics have been proposed in the literature and are listed in Table 1. While this list is not exhaustive, they represent the most commonly used metrics. Selectivity, analogous to the concept of relative volatility used in distillation, is perhaps the most commonly used metric. The selectivity is defined as

$$\alpha = \frac{\left(\frac{\text{equilibrium solid loading of heavy component}}{\text{equilibrium solid loading of light component}}\right)}{\left(\frac{\text{gas phase composition of heavy component}}{\text{gas phase composition of light component}}\right)} \quad (1)$$

Many definitions of selectivity are traditionally used. They mostly differ in the manner in which the equilibrium solid loading is calculated. The Henry selectivity, α_H, is calculated at low concentrations, i.e., at the limit where the adsorption isotherm is linear. For pure component selectivity, α_P, the equilibrium loadings are calculated at the partial pressure corresponding to the feed but without accounting for competitive/co-operative adsorption. For the competitive (or mixture) selectivity, α_C, the solid loadings are calculated

* Corresponding author.
E-mail address: arvind.rajendran@ualberta.ca (A. Rajendran).
[1] Current address: Institute of Process Engineering, ETH Zurich, CH 8092, Switzerland.
[2] Current address: INQUINOA (CONICET), National University of Tucuman, 4000 San Miguel de Tucumán, Argentina.

α_C competitive selectivity [–]
α_H Henry selectivity [–]
α_{pd} rate of pressure change [s^{-1}]
α_P pure-component selectivity [–]
β_C competitive working capacity [$mol\,kg^{-1}$]
β_P pure-component working capacity [$mol\,kg^{-1}$]
ΔU_i internal energy [$J\,mol^{-1}$]
ϵ_b column void fraction [–]
ϵ_p particle voidage [–]
η compression/evacuation efficiency [–]
γ adiabatic constant [–]
γ_A Ackley's figure of merit [$mol\,kg^{-1}$]
γ_N Notaro's figure of merit [$mol\,kg^{-1}$]
γ_W Wiersum's figure of merit[$mol^3\,J^{-1}\,kg^{-2}$]
γ_Y Yang's figure of merit [–]
λ penalty function
μ fluid viscosity [$kg\,m^{-1}\,s^{-1}$]
ψ penalty function
ρ_c crystal density of adsorbent [$kg\,m^{-3}$]
ρ_g density of fluid phase [$kg\,m^{-3}$]
ρ_s particle density of adsorbent [$kg\,m^{-3}$]
ρ_w wall density [$kg\,m^{-3}$]
τ tortuosity [–]

Roman symbols
b_0 adsorption equilibrium parameter for site 1 [$m^3\,mol^{-1}$]
c fluid phase concentration [$mol\,m^{-3}$]
$C_{p,a}$ specific heat capacity of the adsorbed phase [$J\,mol^{-1}\,K^{-1}$]
$C_{p,g}$ specific heat capacity of the gas phase [$J\,mol^{-1}\,K^{-1}$]
$C_{p,s}$ specific heat capacity of the adsorbent [$J\,kg^{-1}\,K^{-1}$]
$C_{p,w}$ specific heat capacity of the column wall [$J\,mol^{-1}\,K^{-1}$]
d_0 adsorption equilibrium parameter for site 2 [$m^3\,mol^{-1}$]
D_L axial dispersion [$m^2\,s^{-1}$]
D_m molecular diffusivity [$m^2\,s^{-1}$]
h_{in} inside heat transfer coefficient [$J\,m^{-2}\,K^{-1}\,s^{-1}$]
h_{out} outside heat transfer coefficient [$J\,m^{-2}\,K^{-1}\,s^{-1}$]
J objective function
k mass transfer coefficient [s^{-1}]
K_w thermal conductivity of column wall [$J\,m^{-1}\,K^{-1}\,s^{-1}$]
K_z effective gas thermal conductivity [$J\,m^{-1}\,K^{-1}\,s^{-1}$]
L column length [m]
n_{comp} number of components
P pressure [Pa]
q concentration in the solid phase [$mol\,kg^{-1}$]
q_{sb} saturation concentration in the solid phase for site 2 [$mol\,kg^{-1}$]
q_{sd} saturation concentration in the solid phase for site 2 [$mol\,kg^{-1}$]
Q mass flow rate [$kg\,s^{-1}$]
R universal gas constant [$m^3\,Pa\,mol^{-1}\,K^{-1}$]
r_{in} inner column radius [m]
r_{out} outer column radius [m]
T temperature [K]
t time [s]
T_a ambient temperature [K]
T_w column wall temperature [K]
ν interstitial velocity [$m\,s^{-1}$]
z bed coordinate [m]

Abbreviations, subscripts and superscripts
i index of component
ADS adsorption step
BLO blowdown step
comp competitive equilibrium
EVAC evacuation step
feed feed condition
FP feed pressurisation step
H high
INT intermediate
L low
LPP light product pressurisation step
out outlet stream
PRESS pressurisation
pure pure-component equilibrium

at the feed composition, but now accounting for competitive/co-operative adsorption. Note that systems that can be described by the single-site Langmuir isotherm have a constant selectivity that is invariant with composition/concentration, i.e., $\alpha_H = \alpha_C$. The major drawback of using selectivity as metric arises from the fact that it does not consider the differences in equilibrium solid phase loading caused by a pressure or temperature swing enforced in an adsorption process. This aspect is critical as it determines the effective amount of gas that could be adsorbed and desorbed from an adsorbent. To account for the regeneration of the adsorbent during a pressure or temperature swing process, the working capacity has been used. The working capacity of an adsorbent is defined as the difference in equilibrium capacities between the high and low pressures for the case of P/VSA and high and low temperature for the case of TSA. Typically the high pressure corresponds to the partial pressure of the components in the feed. The definition of the equivalent quantity for the low pressure for the case of PSA (and the high temperature for TSA) is often not defined clearly. Some practitioners consider the lowest total pressure at a composition of the product or sometimes at the feed composition. Selectivity and the working capacity using the pure component isotherms at a given feed condition have been suggested as adsorbent metrics (Harlick and Tezel, 2004). Note that the definition of either selectivity or working capacity does not take into account the temperature variation associated with the exothermic nature of the adsorption process.

Further to the use of selectivity and working capacity, lumped parameters of selectivity and working capacity were proposed by Notaro et al. (1998), Ackley et al. (2000), Rege and Yang (2001) for a PSA based air separation process. These "figures of merit" (FOM) proposed by Notaro et al. (1998) and Ackley et al. (2000) were defined such that the multi-component equilibrium loadings were evaluated at pressure, temperature and composition corresponding to the adsorption and desorption conditions rather than a single point loading used in the calculation of selectivity and working capacity discussed above. The figure of merit proposed by Rege and Yang (2001) was a simplified form of the figure of merit proposed by Notaro et al. (1998). The metric accounted for the working capacity of both the heavy and the light species rather than just the heavy species as was the case with Notaro et al. (1998). Yang's FOM was applied for an air separation process and was shown to have a direct correlation with purity, recovery or product throughput if two of these indicators were fixed.

A simplified model for rapid adsorbent screening was recently put forward by Maring and Webley (2013). In this model a simple cycle was simulated by assuming the adsorption column to be a batch system, i.e., in the absence of axial gradients. This effectively

Table 1
Definition of adsorbent metrics and the comparison of these metrics calculated at 25 °C for different adsorbents considered in this study. The underlined value represents the adsorbent that is ranked best by the specific metric. The equilibrium loadings at adsorption and desorption conditions are $q^*_{ads} = q^*$ (1 bar, 298.15 K, y_{feed}) and $q^*_{des} = q^*$ (0.03 bar, 298.15 K, y_{feed}), respectively.

Adsorbent metric	Definition	Adsorbents				References
		Mg-MOF-74	Zeolite 13X	UTSA-16	CS-AC	
CO_2 adsorption capacity [mmol g^{-1}]	$q^*_{ads,pure}\big\vert_{feed}$	6.36	3.44	2.33	0.90	(Yang, 1997)
Henry selectivity [-]	$\alpha_H = \dfrac{H_{CO_2}}{H_{N_2}} = \dfrac{(q_{sb}b + q_{sd}d)_{CO_2}}{(q_{sb}b + q_{sd}d)_{N_2}}$	385.80	834.41	374.84	18.12	(Knaebel, 1995)
Pure-component selectivity [-]	$\alpha_P = \left[\left(\dfrac{q^*_{CO_2,pure}}{q^*_{N_2,pure}}\right)\dfrac{y_{N_2}}{y_{CO_2}}\right]\Big\vert_{feed}$	45.49	69.82	200.62	17.99	(Yang, 1997)
Competitive selectivity [-]	$\alpha_C = \left[\left(\dfrac{q^*_{CO_2,comp}}{q^*_{N_2,comp}}\right)\dfrac{y_{N_2}}{y_{CO_2}}\right]\Big\vert_{feed}$	404.08	981.45	374.84	60.55	(Yang, 1997)
Pure-component working capacity [mmol g^{-1}]	$\beta_{P_i} = \left(q^*_{ads,pure} - q^*_{des,pure}\right)\big\vert_{feed}$	2.07	1.04	1.59	0.64	(Yang, 1997)
Competitive working capacity [mmol g^{-1}]	$\beta_{C_i} = \left(q^*_{ads,comp} - q^*_{des,comp}\right)\big\vert_{feed}$	2.05	1.03	1.58	0.51	(Yang, 1997)
Notaro's FOM [mol kg^{-1}]	$\gamma_N = \beta_{C_{CO_2}}\left(\dfrac{\alpha^2_{C_{ads}}}{\alpha_{C_{des}}}\right)$	866.00	1189.12	594.15	68.17	(Notaro et al., 1998)
Ackley's FOM [mol kg^{-1}]	$\gamma_A = \beta_{C_{CO_2}}\left(\dfrac{\beta_{P_{CO_2}}}{\beta_{P_{N_2}}}\right)$	5.52	4.01	39.59	1.21	(Ackley et al., 2000)
Yang's FOM [-]	$\gamma_Y = \alpha_C\left(\dfrac{\beta_{P_{CO_2}}}{\beta_{P_{N_2}}}\right)$	1089.08	3794.59	9362.28	144.36	(Rege and Yang, 2001)
Wiersum's FOM [mol^3 J^{-1} kg^{-2}]	$\gamma_W = \dfrac{(\alpha_C - 1)^{0.5}\beta^2_{C_{CO_2}}}{\left\vert\Delta H_{ads_{CO_2}}\right\vert}$	2.71	0.87	1.26	0.04	(Wiersum et al., 2013)

simplified the constitutive partial differential equations to ordinary differential equations. Using this model, the authors studied various parameters that affect process performance. The simplified model was able to capture the equilibrium effects along with the heat effects which were absent in the equilibrium theory models. These models were developed for a given cycle configuration, hence they overcame the limitation of the absence of cycle configuration in simple adsorbent metrics.

Adsorbent screening using molecular modelling has been used in the recent years. In one of the recent studies (Yazaydin et al., 2009), the screening of 14 different metal organic frameworks (MOFs) was performed using Monte Carlo simulations. The different MOFs were ranked using the uptake rates at feed conditions (0.1 bar and room temperature). The parasitic energy due to CCS is important and it is ultimately one of the deciding factors for an adsorbent material or process to be used on a commercial scale. Recently, a parasitic energy curve was proposed (Lin et al., 2012), which relates the parasitic energy with the Henry coefficient (adsorption equilibrium constant in the Langmuir isotherm model) of CO_2. Thousands of hypothetical materials were generated using Monte Carlo simulations. For each of these materials, optimal process conditions to minimise the parasitic energy were evaluated using a hybrid pressure and temperature swing adsorption cycle. The major shortcoming of this approach stems from the fact that the material selection process is approached using the CO_2 Henry coefficient alone. In this study, although the effect of N_2 was accounted for in the definition of the adsorption equilibria, the effect of N_2 on the parasitic energy was not fully addressed.

Simulations of adsorption processes involve the solution of coupled algebraic and partial differential equations that are complex and time consuming. Further, explicit design-methods are established only for simple processes under limiting conditions of isothermal operation along with the assumption of local equilibrium. Hence, adsorbent metrics were developed to overcome the limitations and to provide researchers a simple tool to identify promising adsorbents. It is important to note that most metrics and simplified models do not take into account mass and heat transfer effects, cycle configurations, pressure drop effects and the

characteristics of wave dynamics that occur during adsorption and desorption operations. Further, most of the metrics were developed for raffinate cycles, i.e., separations where the light component was the target product. Finally, it is still not clear which process performance, e.g. purity, recovery, energy, etc., the adsorbent metrics correlate to. Over the years adsorbent metrics have been used as the de-facto measure to make claims that one adsorbent is better than the other. This trend is noticed particularly in the area of CO_2 capture that has spurred the development of hundreds of new materials.

The main goal of this paper is to revisit these adsorbent metrics and ask a key question "Can these adsorbent metrics be reliably used to screen adsorbents?". This important question is answered by considering the case of post-combustion CO_2 capture, a topic that has occupied the interest of both synthetic chemists and engineers. We consider four adsorbent materials, the properties of which have been reported in the literature. In order to answer the question, we use detailed models that have been demonstrated to predict pilot scale operations and cycle optimisation which allows the thorough search for thousands of operating conditions, thereby allowing the adsorbent to "choose" operating conditions that maximise its ability.

2. Case study

2.1. Post-combustion capture of CO_2

In this case study, CO_2 capture from a dry post-combustion flue gas stream is considered. The actual flue gas from a coal-based power plant predominantly consists of CO_2 and N_2 along with trace quantities of impurities like SO_x, NO_x and moisture. The impurities present in the flue gas will compete with CO_2 for the sites available for adsorption. Presence of certain impurities might also degrade the adsorbents over a period of time. For polar adsorbents like Zeolite 13X, the affinity of water can be many times higher than that of CO_2. Although these impurities will have an impact on the process performance, we have assumed the flue gas to be composed of 15% CO_2 and 85% N_2 available at 1 bar pressure and

Table 2
Dual-site Langmuir isotherm parameters for CO_2/N_2 on Mg-MOF-74, Zeolite 13X, UTSA-16, CS-AC and the three hypothetical materials studied in this work.

		$q_{sb,i}$ [mol kg^{-1}]	$q_{sd,i}$ [mol kg^{-1}]	$b_{0,i}$ [m^3 mol^{-1}]	$d_{0,i}$ [m^3 mol^{-1}]	$-\Delta U_{b,i}$ [kJ mol^{-1}]	$-\Delta U_{d,i}$ [kJ mol^{-1}]
Mg-MOF-74	CO_2	6.80	9.90	1.81×10^{-07}	1.06×10^{-06}	39.30	21.20
	N_2	14.00	–	3.45×10^{-06}	–	15.50	–
Zeolite 13X	CO_2	3.09	2.54	8.65×10^{-07}	2.63×10^{-08}	36.60	35.70
	N_2	5.84	–	2.50×10^{-06}	–	15.80	–
UTSA-16	CO_2	5.00	3.00	6.24×10^{-07}	1.87×10^{-23}	30.60	44.70
	N_2	12.70	–	2.96×10^{-06}	–	9.77	–
CS-AC	CO_2	0.59	7.51	9.40×10^{-06}	1.04×10^{-05}	25.61	17.55
	N_2	0.16	41.30	1.81×10^{-03}	1.72×10^{-12}	8.67	44.90
Adsorbent A	CO_2	6.80	9.90	1.81×10^{-07}	1.06×10^{-06}	39.30	21.20
	N_2	12.70	–	2.96×10^{-06}	–	9.77	–
Adsorbent B	CO_2	6.80	9.90	1.81×10^{-07}	1.06×10^{-06}	39.30	21.20
	N_2	12.70	–	3.95×10^{-04}	–	9.77	–
Adsorbent C	CO_2	6.80	9.90	1.05×10^{-09}	6.19×10^{-09}	39.30	21.20
	N_2	12.70	–	2.96×10^{-06}	–	9.77	–

25 °C. The assumption on the flue gas components would simplify the process and would allow us to provide key insights regarding the performances of different material(s) for the questions posed in this work. If the performances of the adsorbent materials are found to be attractive, sensitivity of impurities on such materials can be examined in the future.

Previous studies from our group and in the literature (Zhang and Webley, 2008; Haghpanah et al., 2013a) have clearly identified the advantage of vacuum swing adsorption over pressure swing adsorption and hence this study considers only VSA based CO_2 capture. In order to evaluate the adsorbent metrics, four different adsorbents are considered; Zeolite 13X, two metal organics frameworks (MOFs) and a type of activated carbon. Zeolite 13X is the current benchmark material for CO_2 capture. Zeolite 13X has high CO_2/N_2 selectivity and has been shown to achieve purity–recovery in excess of 90% in both simulations (Zhang and Webley, 2008; Haghpanah et al., 2013b) and in pilot scale demonstrations (Krishnamurthy et al., 2014). Metal organic frameworks have caught recent attention for their high CO_2 adsorption capacity and selectivity (Zhang et al., 2014). Two MOFs, namely, Mg-MOF-74 and UTSA-16 were chosen as representative materials. The stability of these materials is still being explored, and large-scale demonstrations have not been reported. However this should not distract the study of these materials to evaluate their potential. Carbonaceous materials like activated carbon are moisture-tolerant and less expensive when compared to other adsorbents (Radosz et al., 2008). This makes them a potential candidate for study. In this work a specific coconut shell activated carbon, henceforth called CS-AC, reported by Xu et al., (Xu et al., 2011) is used. This granular material has a BET surface area of 921.7 m^2/g, a total pore volume of 0.37 cm^3/g and a nominal pore size of 0.73 nm. The adsorption mechanism for all the four adsorbents considered in this study were based on physical adsorption and the separation mechanism was equilibrium-based.

2.2. Adsorption equilibria

The equilibrium isotherm data for CO_2 and N_2 on Zeolite 13X were measured in our laboratory (Haghpanah et al., 2013b) while the isotherms for Mg-MOF-74, UTSA-16 and CS-AC were obtained from the literature (Xiang et al., 2012; Maring and Webley, 2013). The adsorption equilibria for the four adsorbents were described using a dual-site Langmuir (DSL) model:

$$q_i^* = \frac{q_{sb,i} b_i c_i}{1 + \sum_{i=1}^{n_{comp}} b_i c_i} + \frac{q_{sd,i} d_i c_i}{1 + \sum_{i=1}^{n_{comp}} d_i c_i} \quad (2)$$

where $q_{sb,i}$ and $q_{sd,i}$ are the solid-phase saturation loadings for the two sites, and b_i and d_i were the adsorption equilibrium constants which followed an Arrhenius-type temperature dependence given by

$$b_i = b_{0,i} e^{\left(-\frac{\Delta U_{b,i}}{RT}\right)} \quad (3a)$$

$$d_i = d_{0,i} e^{\left(-\frac{\Delta U_{d,i}}{RT}\right)} \quad (3b)$$

The isotherm parameters for the adsorbents are given in Table 2 and the fitted pure component isotherms at 25 °C are shown in Fig. 1. From the pure component isotherms, it was clear that the adsorption capacity of CO_2 on Mg-MOF-74 was the highest among the four adsorbents, followed by Zeolite 13X, UTSA-16 and CS-AC. For the case of Mg-MOF-74, higher CO_2 adsorption capacity was also accompanied by higher N_2 adsorption. CS-AC had the least
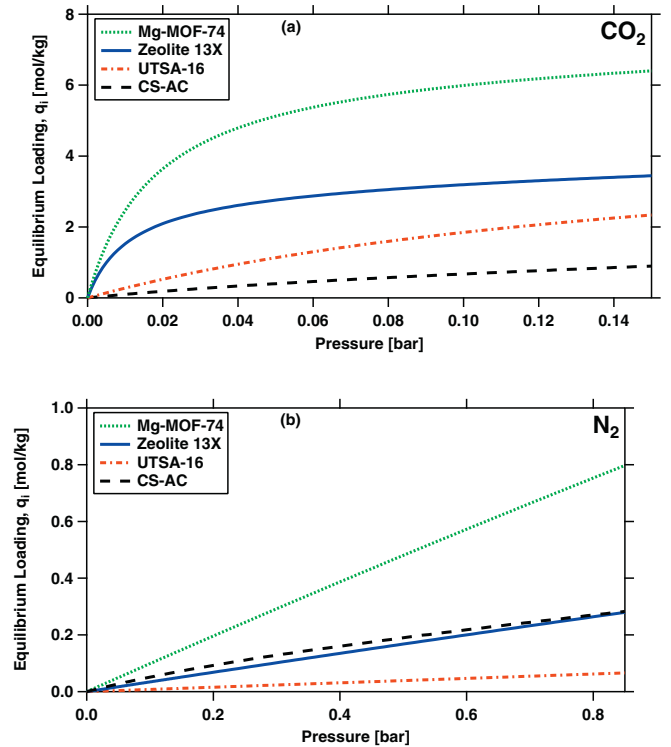

Fig. 1. Single component isotherms for (a) CO_2 and (b) N_2 at 25 °C on the four materials studied.

non-linearity for CO_2 but was accompanied by a stronger N_2 adsorption compared to Zeolite 13X and UTSA-16.

The adsorbent metrics calculated for the different adsorbents are summarised in Table 1. The ranking of adsorbents using different metrics paint an interesting picture. All adsorbent metrics consistently ranked CS-AC as the least favourable. However, there is no clear winner predicted by the adsorbent metrics. Mg-MOF-74 is predicted as the most favourable by four metrics, while Zeolite 13X and UTSA-16 are each, ranked as the best by three metrics. Hence, it becomes difficult to rank Mg-MOF-74, Zeolite 13X and UTSA-16 due to discrepancy in the ranking provided by various adsorbent metrics. It now becomes pertinent to examine which of these materials offers the best separation performance.

3. Adsorption process design and optimisation

3.1. Modelling of the adsorption process

In order to evaluate the efficacy of the adsorbent metrics, it is important to evaluate the adsorbent performance under realistic process conditions. For this a detailed model is developed. The adsorption dynamics in the column is described using a one dimensional mathematical model. The transport equations, a set of coupled non-linear partial differential equations, and the boundary conditions necessary to solve the equations are summarised in the supplementary material. The model assumes an axially dispersed plug flow behaviour to represent the gas flow through the fixed bed. The model assumes ideal gas behaviour and local thermal equilibrium between the gas and the solid phase. Energy balance equations for the bed and the column wall take into account the dispersive and convective effects to accurately describe the heat transfer. The pressure drop in the column is considered. Zeolite 13X used in this study is pelletised using a binder and properties of the pellets formed are used in the cycle simulations. For the MOFs, experimental equilibrium data are available only for the crystals and not for particles. Hence, it was assumed that pellets can be formed without loss in capacity and the equilibrium data for "pseudo" particles was assumed to be identical to the crystals on a "per unit mass" basis. We assume that the crystals are formed as particles without the use of binders. This is akin to the concept of binderless particles which is now commonly reported in the zeolite and MOF literature (Finsy et al., 2009; Silva et al., 2012; Schumann et al., 2012). These reports indicate that the particle formation process introduces macroporosity, in addition to the micropores that are present in the crystal. Accordingly, MOF particles were assumed to be formed from pure crystals with a particle voidage of 0.35 (sample calculation shown in supporting information), which was then used in the process simulations. The controlling mass transfer mechanism in Zeolite 13X has been established to be controlled by molecular diffusion in the macropores (Hu et al., 2014). There is no mass transfer study available on the MOF materials. Under this situation it was assumed that the molecular diffusion in the macropores also controls the mass transfer in the other materials as well. Note that all adsorbents studied here separate CO_2 and N_2 based on equilibrium properties. Hence the description of the mass transfer, although important, is expected to have a minor impact on process performance. This has been confirmed by simulations that are not reported here. When adsorbent properties of Mg-MOF-74, UTSA-16 and CS-AC were unavailable, properties of Zeolite 13X were used for the cycle simulations. The adsorbent properties and the bed voidage was assumed to be uniform across the column and are listed in Table 3.

For all the cycle simulations reported in this work, the bed was initially saturated with pure N_2 at 1 bar and 25 °C. As discussed in Haghpanah et al. (2013a), a finite volume technique

Table 3
Simulation parameters used in PSA cycle modelling for the four materials studied.

Parameter	Value
Column properties	
Column length, L [m]	1.00
Inner column radius, r_{in} [m]	0.1445
Outer column radius, r_{out} [m]	0.1620
Column void fraction, ϵ_b [−]	0.37
Particle voidage, ϵ_p [−]	0.35
Particle radius, r_p [m]	7.5×10^{-4}
Tortuosity, τ [−]	3.00
Fluid and adsorbent properties	
Flue gas pressure, P_{feed} [bar]	1.00
Feed temperature, T_{feed} [K]	298.15
Ambient temperature, T_a [K]	298.15
Column wall density, ρ_w [kg m^{-3}]	7800
Particle density, ρ_s [kg m^{-3}]	
Mg-MOF-74	588.25
Zeolite 13X	1130.00
UTSA-16	1092.00
CS-AC	799.50
Specific heat capacity of fluid phase, $C_{p,g}$ [J mol^{-1} K^{-1}]	30.70
Specific heat capacity of adsorbed phase, $C_{p,a}$ [J mol^{-1} K^{-1}]	30.70
Specific heat capacity of adsorbent, $C_{p,s}$ [J kg^{-1} K^{-1}]	
Mg-MOF-74	896.00
Zeolite 13X	1070.00
UTSA-16	1070.00
CS-AC	1070.00
Specific heat capacity of column wall, $C_{p,w}$ [J kg^{-1} K^{-1}]	502.00
Fluid viscosity, μ [kg m^{-1} s^{-1}]	1.72×10^{-5}
Molecular diffusivity, D_m [m^2 s^{-1}]	1.30×10^{-5}
Adiabatic constant, γ [−]	1.40
Effective gas thermal conductivity, K_z [J m^{-1} K^{-1} s^{-1}]	0.09
Thermal conductivity of column wall, K_w [J m^{-1} K^{-1} s^{-1}]	16.00
Inside heat transfer coefficient, h_{in} [J m^{-2} K^{-1} s^{-1}]	8.60
Outside heat transfer coefficient, h_{out} [J m^{-2} K^{-1} s^{-1}]	2.50
Compression/evacuation efficiency, η [−]	0.72
Universal gas constant, R [m^3 Pa mol^{-1} K^{-1}]	8.314

using a van-Leer flux limiter (van Leer, 1979; LeVeque, 2002) was used to discretise the system of coupled non-linear partial differential equations into 30 volume elements in the axial direction. The resulting ordinary differential equations (ODE) were integrated using a stiff solver available in MATLAB. The performance indicators, namely purity, recovery, energy and productivity were calculated once the system attained cyclic steady state (CSS). The system was considered to have reached CSS if the mass balance error for five consecutive cycles was less than 0.5%. A maximum of 2000 cycles was set for each combination of operating conditions to attain CSS. It is to be noted that for the cycle simulations, a single column was made to undergo the constitutive steps of a cycle in a specified sequence. When there were coupled steps in the process, the output variables from a step namely, fluid phase and solid phase concentrations, the bed temperatures and the pressure across the column were stored in a data buffer. The data stored in the buffer was used as an input for the coupled step for further simulations. It is worth noting that this is a standard practice in adsorption process simulation. The number of columns required to implement the cycles depends on the duration of each step and the nature of interconnected steps. Translating a single column design to a multi-column configuration can change the value of productivity as idle steps may be required. However, other performance metrics such as purity, recovery and energy consumption will not be affected.

The full cycle model used in this work has been shown to successfully predict multi-column pilot scale experiments reported elsewhere (Krishnamurthy et al., 2014). The transient profiles and the performance indicators namely, purity, recovery, energy consumption and productivity obtained from the pilot scale experiments were comparable to the results obtained from numerical
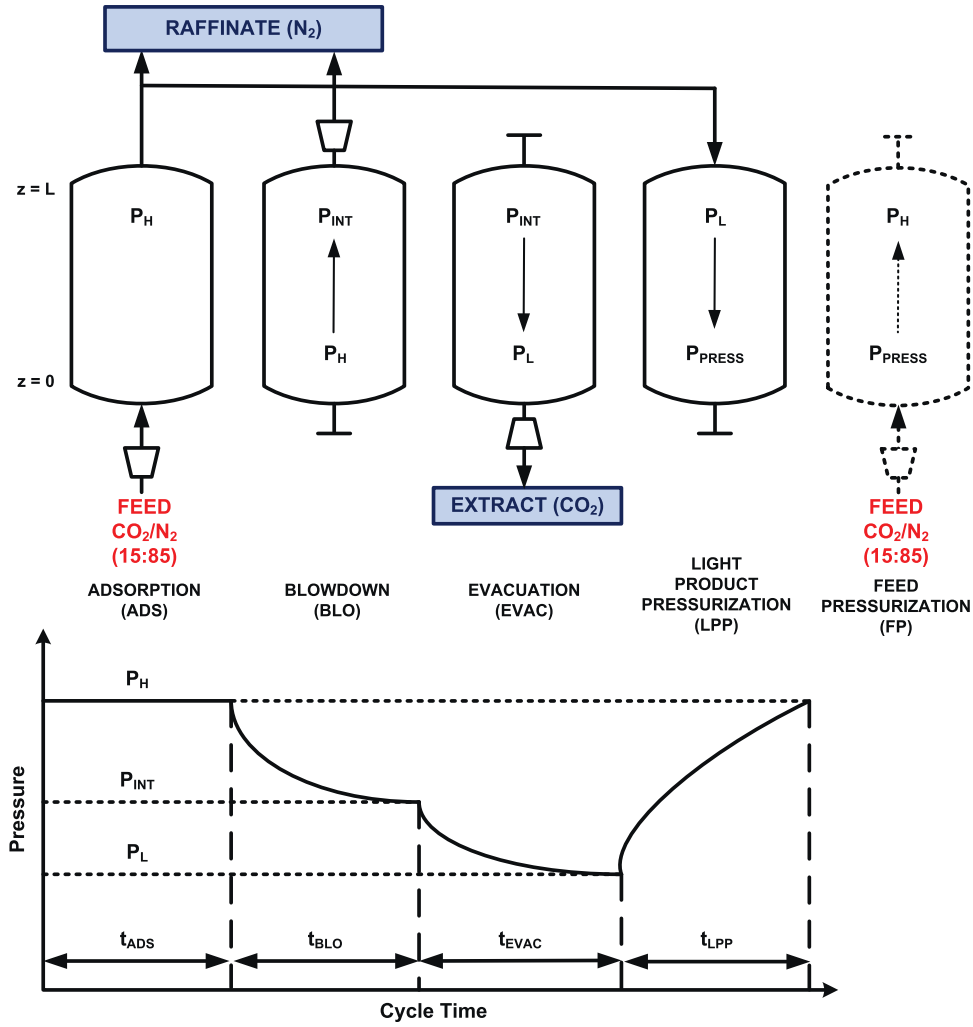
Fig. 2. Process schematic for a 4-step cycle with light product pressurisation (LPP).

simulations using the full cycle model. Hence, we have confidence in using these models for adsorbent screening.

3.2. Cycle configuration

In this work a 4-step PSA cycle with a light product pressurisation (LPP), shown in Fig. 2 is used. This configuration is chosen based on previous optimisation work that showed that the 4-step cycle with LPP was superior compared to many others achieving target purity and recovery at the lowest energy consumption (Haghpanah et al., 2013b). The 4-step PSA cycle with LPP consists of the following steps:

1. **Adsorption (ADS):** Feed gas is introduced at $z=0$ at the feed pressure (P_{feed}) and temperature (T_{feed}). The strongly adsorbing component (CO_2) adsorbs preferentially over the weakly adsorbing component (N_2) in this step. The end, $z=L$ is kept open and a N_2 rich product is collected at this end.
2. **Blowdown (BLO):** The feed end of the column ($z=0$) is closed and the column is depressurised from high pressure (P_H) to an intermediate pressure (P_{INT}) from the $z=L$ end. This step removes the N_2 from the column, thereby increasing the concentration of CO_2 in the column. Due to depressurisation, a small amount of CO_2 could be lost from the N_2 product end.

3. **Evacuation (EVAC):** CO_2 concentrates near $z=0$ and in order to remove the product, the column is closed at the end, $z=L$ and is depressurised from an intermediate pressure (P_{INT}) to a low pressure (P_L).
4. **Light product pressurisation (LPP):** In this step, the feed end, i.e., $z=0$ is closed and the column is pressurised in the reverse direction, i.e., $z=L$ using the light product obtained from the adsorption step. The LPP step is limited by the high pressure (P_H) in the column and once the desired high pressure in the column is reached, the adsorption outlet stream is collected as a raffinate product. If the stream from the adsorption step is not sufficient to pressurise the column to the high pressure, an additional feed pressurisation step is introduced after the maximum duration of the LPP step is reached, which is set as the time of adsorption step (t_{ADS}). This step serves to compress the CO_2 tail that is formed during the blowdown step and improves CO_2 recovery (Haghpanah et al., 2013b).

3.3. Optimisation framework

In this work, similar to the previous studies, genetic algorithm (GA) is used to optimise the process. Two separate problems are studied. The first one deals with an unconstrained optimisation problem of simultaneously maximising purity and recovery. The second problem deals with maximisation of productivity and

minimisation of energy subject to constraints on purity and recovery. The objectives are defined as follows:

Purity, Pu [%]

$$= \frac{\text{Total moles of } CO_2 \text{ in the extract product}}{\text{Total moles of } CO_2 \text{ and } N_2 \text{ in the extract product}} \times 100 \tag{4a}$$

Recovery, Re [%]

$$= \frac{\text{Total moles of } CO_2 \text{ in the extract product}}{\text{Total moles of } CO_2 \text{ fed into the cycle}} \times 100 \tag{4b}$$

Energy, En $\left[\dfrac{\text{kWh}}{\text{tonne } CO_2 \text{ captured}}\right]$

$$= \frac{E_{ADS} + E_{BLO} + E_{EVAC} + E_{FP}}{\text{Mass of } CO_2 \text{ in the extract product per cycle}} \tag{4c}$$

Productivity, Pr $\left[\dfrac{\text{mol } CO_2}{\text{m}^3 \text{ adsorbent.s}}\right]$

$$= \frac{\text{Total moles of } CO_2 \text{ in the extract product}}{(\text{Total volume of adsorbent})(\text{Cycle time})} \tag{4d}$$

where E_j refers to the energy consumption in step j. The energy consumption (E_j) for the vacuum pumps used in the blowdown and evacuation steps with a delivery pressure of 1 bar is given by

$$E = \frac{1}{\eta} \frac{\gamma}{\gamma - 1} \int_{t=0}^{t=t_{step}} QP_{out} \left[\left(\frac{1}{P_{out}}\right)^{\frac{(\gamma-1)}{\gamma}} - 1 \right] dt \tag{5}$$

where P_{out} is the intermediate or low pressure for the blowdown and evacuation step, respectively, Q is the total gas flow rate and η, is the efficiency of the vacuum pump.

For the optimisation problem, the step times for adsorption, blowdown and evacuation; the intermediate and the low pressures; and the feed velocity were considered as decision variables. It is well known that GA does not guarantee a global minimum but has the ability to escape local minima. Genetic algorithm can be easily coupled with the full model for the adsorption process as described in the literature (Haghpanah et al., 2013a). GA is also amenable to parallelisation and helps to speed-up the optimisation. A non-dominated sorting genetic algorithm proposed by Deb et al. (2002) available in the MATLAB global optimisation toolbox along with the MATLAB parallel computing toolbox was used in this work. All computations reported in this work were carried out on a desktop workstation with two 12-core INTEL Xeon 2.5GHz processors and 128GB RAM. The GA uses 50 generations with a population size of 24 times the number of decision variables for the multi-objective optimisation routines. The larger population size comes at the cost of longer computation times, but allows the optimiser to thoroughly search the entire decision variable space which enabled the optimiser to escape local minima.

4. Results and discussions

4.1. Maximisation of purity and recovery

One of the main challenges in adsorptive CO_2 capture is the requirement to concentrate the CO_2 composition from 15 mol% to >90% in the product while achieving a CO_2 recovery in excess of 90%. The constraints on purity arise from sequestration requirements and those on recovery are imposed by regulatory bodies such as the U.S. Department of Energy. Hence, it is important that no matter which adsorbent is used, these constraints should be met simultaneously. The four materials considered in this work were subjected to a multi-objective optimisation in order to maximise purity and
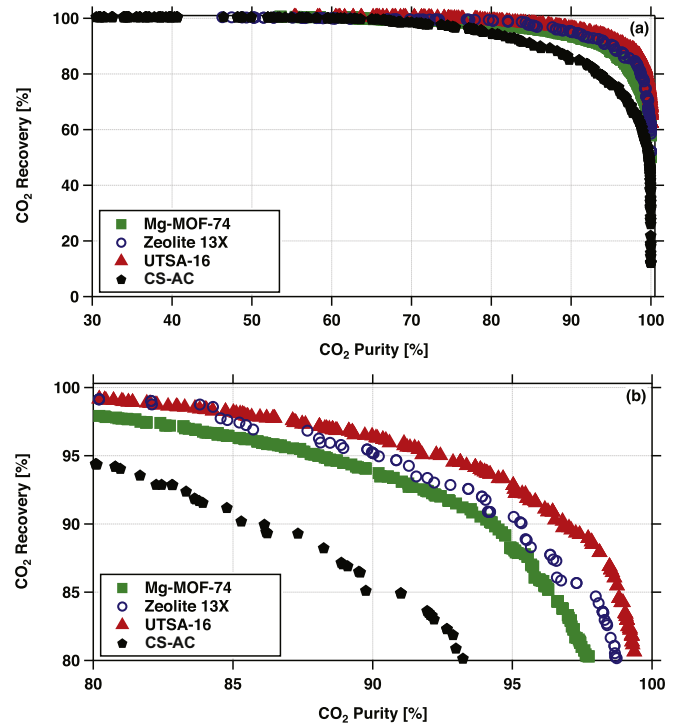

Fig. 3. (a) CO_2 purity–recovery Pareto curves for the four materials studied in this work. The Pareto curves are plotted on a magnified axis in (b) for clarity.

recovery. The objective functions for the optimisation were defined as

$$\min J_1 = \frac{1}{Pu_{CO_2}} \tag{6a}$$

$$\min J_2 = \frac{1}{Re_{CO_2}} \tag{6b}$$

The decision variables t_{ADS}, t_{BLO} and t_{EVAC} were varied between 20 and 100 s, 30 and 200 s and 30 and 200 s, respectively; P_{INT} and P_L were varied between 0.03 and 0.50 bar; and v_0 was varied between 0.1 and 2 m s^{-1}. The lowest pressure for the vacuum pump, 0.03 bar, comes from our experience in operating pilot scale units (Krishnamurthy et al., 2014) and from previous studies (Haghpanah et al., 2013a,b) that point to the fact that reducing vacuum pressures to lower values result in increased energy consumption. In order to make the process meaningful the constraint, $P_{INT} \geq P_L$, was imposed.

The Pareto curve for purity–recovery optimisation for the four materials is shown in Fig. 3. The Pareto curve provides the "best" trade-off that is achievable for each material. The region to the top-right of each curve is unattainable for the operating range provided; while the region to the bottom-left is sub-optimal. Hence, an ideal process operation is one that lies on the Pareto curve. Also note that on the Pareto curve, an increase in one of the performance indicators results in lowering the other. As seen from the figure, Mg-MOF-74, Zeolite 13X and UTSA-16 were able to achieve purity and recovery in excess of 90% while the CS-AC was not able to achieve these targets. Further, over the entire range of purity and recovery the performance of the four materials can be ranked as UTSA-16 > Zeolite 13X > Mg-MOF-74 > CS-AC. The poor performance of CS-AC was in fact predicted by all metrics. This could be explained by the fact that CS-AC has both a weak CO_2 adsorption and a strong N_2 adsorption, i.e, a selectivity that is too low compared to the other materials. The Pareto curves of the other three materials, although clearly distinct from one-another are reasonably close to
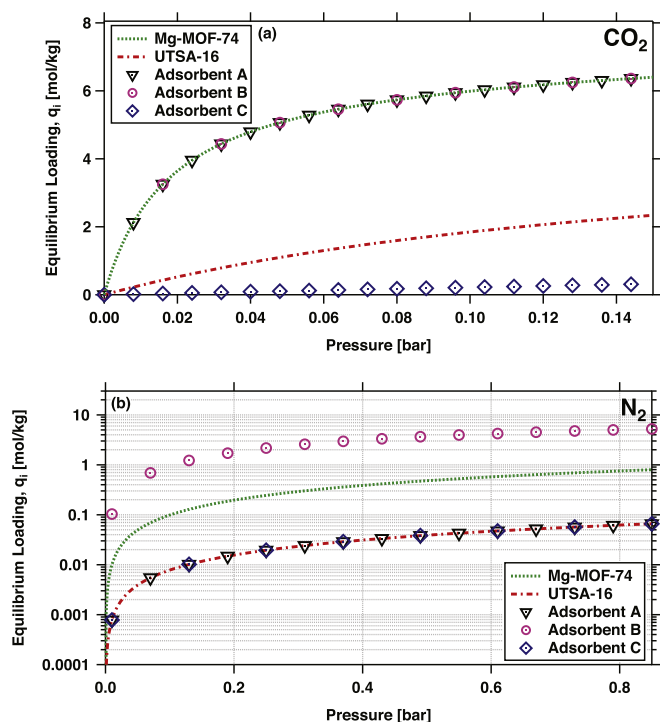
Fig. 5. CO_2 purity–recovery Pareto curves for Mg-MOF-74, UTSA-16, and three hypothetical adsorbents.

Fig. 4. Single component isotherms for (a) CO_2 and (b) N_2 at 25 °C on Mg-MOF-74, UTSA-16 (solid lines) and three hypothetical adsorbents (open symbols). Note that N_2 isotherms are plotted on a semi-log scale.

each other. The GA is a stochastic optimisation routine and minor deviations in the Pareto curves are normally seen. The Pareto curves shown here were obtained by taking the best points from various optimisation routines with different initial populations. In all cases the relative position of Pareto curves for the different materials was unchanged. At this point it is pertinent to compare the adsorbent metrics to the Pareto curves. Of all the metrics only pure selectivity and Yang's FOM seem to predict the trend correctly. Although they rank the adsorbents correctly the magnitudes of these metrics deserve attention. The pure component selectivity of UTSA-16 is 2.87 times that of Zeolite 13X and 4.41 times that of Mg-MOF-74. Similarly, Yang's FOM for UTSA-16 is 2.47 times larger than Zeolite 13X and 8.60 times larger than that of Mg-MOF-74. However the optimisation results indicate that the advantage of one material over the other, baring CS-AC, is at best marginal.

4.1.1. Importance of N_2 adsorption

In order to understand the effect of selectivity and shape of the isotherm on the process performance, hypothetical adsorbents with different CO_2/N_2 isotherms were chosen and were subjected to a multi-objective optimisation to maximise purity and recovery. Three hypothetical adsorbents were considered such that two adsorbents (A and B) had the same CO_2 isotherm parameters as Mg-MOF-74 and two adsorbents (A and C) had the same N_2 isotherm parameters as UTSA-16. CO_2 and N_2 isotherm parameters on the three hypothetical materials are given in Table 2 and the isotherms are shown in Fig. 4. The Henry selectivity for A, B and C were 4913.91, 36.81 and 28.59, respectively.

The purity–recovery Pareto curves for the three hypothetical adsorbents, Mg-MOF-74 and UTSA-16 are shown in Fig. 5. Adsorbents A, UTSA-16 and C which all had identical N_2 isotherms but different CO_2 isotherms resulted in purity–recovery Paretos that were very close to each other. This indicates that CO_2 affinity is so strong that a change in CO_2 affinity has only a marginal impact on the achievable purity–recovery. At this point it is worth clarifying
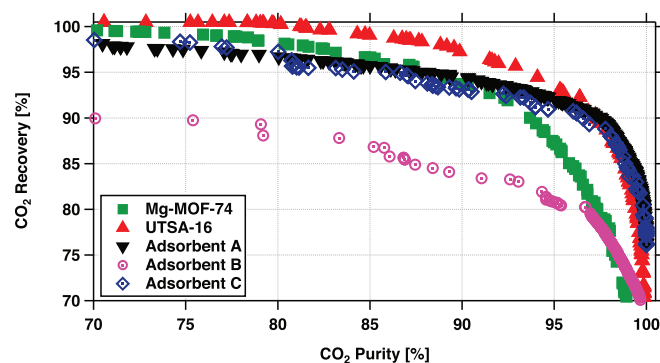
that should CO_2 affinity have been weaker than the isotherms used for material C, then CO_2 is expected to have a decisive impact on process performance (Rajagopalan, 2015). Now let us observe the difference between adsorbents A, Mg-MOF-74 and B, which all had identical CO_2 isotherms but different N_2 isotherms. While adsorbents A and Mg-MOF-74 had similar Pareto curves, adsorbent B with a stronger N_2 affinity showed a Pareto curve that was inferior to all the adsorbents. It is worth noting that even when the Henry selectivity for adsorbents B and C were similar, adsorbent C performed better than adsorbent B. This trend could be explained by considering the N_2 isotherms for the two materials. In the range of working pressures, N_2 isotherm on adsorbent B was sharper than adsorbent C, which contributed to a better performance for adsorbent C.

The analysis with the hypothetical isotherms shows that for an adsorbent which was reasonably selective to CO_2, increasing the CO_2 affinity further does not lead to an improvement in the achievable purity–recovery but it is the N_2 affinity that controls the process performance. This reinforces similar observations reported in the literature (Maring and Webley, 2013) and provides an important insight into the factors that need to be considered during adsorbent synthesis. In other words, synthesising materials that have a lower N_2 affinity might be more beneficial compared to those that have improved CO_2 affinity.

4.2. Minimisation of energy and maximisation of productivity

In the previous section, we have assessed the performance of the four materials based on their purity–recovery Pareto curves. While the purity–recovery Pareto curves provide information about the ability of these adsorbents to meet regulatory requirements they do not provide any information regarding the capital and operating expenses that could be incurred. It is common practice to use productivity and energy consumption as a proxy for capital and operating expenses. Converting these values to cost is a rather complex exercise and is beyond the scope of this work (Susarla et al., 2015). The material used for a given separation process must have the least energy consumption with the maximum productivity for a given volume of adsorbent. Hence, the adsorbents which met the purity–recovery requirements, i.e. in excess of 90% were subjected to an optimisation to obtain the trade-off between the energy consumption and the productivity. The materials considered for the energy-productivity were Mg-MOF-74, Zeolite 13X and UTSA-16, while CS-AC, which did not achieve purity and recovery in excess of 90%, was not considered.

The energy-productivity optimisation was a constrained optimisation problem. Hence, the constraints on the purity–recovery
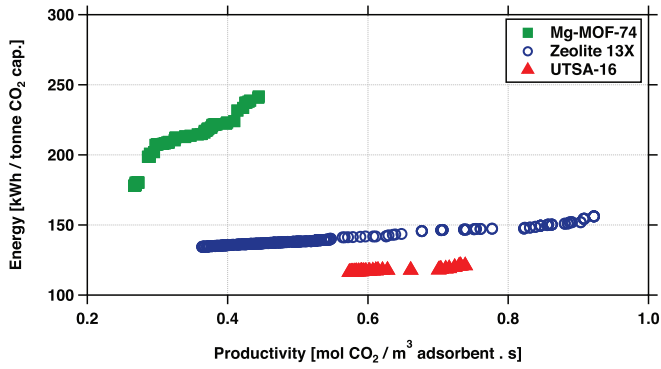
Fig. 6. Energy-productivity Pareto curves for Mg-MOF-74, Zeolite 13X and UTSA-16 that meet 90% purity–recovery constraints.

had to be accounted for in the definition of the objective function that is defined as

$$\min J_1 = \psi_1 E + \lambda_1 \left[\max \left(0, Pu_{\text{target}} - Pu_{CO_2} \right) \right]^2$$
$$+ \lambda_2 \left[\max \left(0, Re_{\text{target}} - Re_{CO_2} \right) \right]^2 \tag{7a}$$

$$\min J_2 = \frac{\psi_2}{Pr} + \lambda_1 \left[\max \left(0, Pu_{\text{target}} - Pu_{CO_2} \right) \right]^2$$
$$+ \lambda_2 \left[\max \left(0, Re_{\text{target}} - Re_{CO_2} \right) \right]^2 \tag{7b}$$

where ψ_i and λ_i were the penalty functions, Pu_{target} and Re_{target} were the target purity and recovery, respectively. The bounds on the decision variables used for the purity–recovery optimisation discussed in the previous section were kept unchanged.

The energy-productivity Pareto obtained from the optimisation is shown in Fig. 6. All the points in the Pareto curve correspond to different sets of operating conditions which met the purity–recovery constraints. The Pareto curves of the three materials show a clear distinction and ranked the materials in the following order: UTSA-16 > Zeolite 13X > Mg-MOF-74; a trend that was observed in the purity–recovery optimisation. The differences in the performances could be explained by examining the decision variables corresponding to the Pareto points. The process configuration includes two vacuum pumps and a blower that contribute to the energy consumption. The contribution from the vacuum pumps is decisive in lowering the energy consumption for a given material or a given process. From Eq. (5), it is clear that the energy consumption depends on the pressure levels between which the vacuum pump operates and the gas flow rate through the vacuum pump. A higher value of P_{out} would result in a lower energy consumption for a vacuum pump. In Fig. 7,
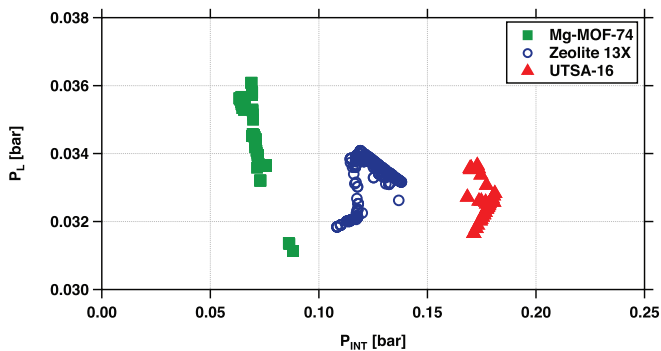

Fig. 7. Intermediate pressure (P_{INT}) and low pressure (P_L) corresponding to the Pareto points for Mg-MOF-74, Zeolite 13X and UTSA-16 shown in Fig. 6.
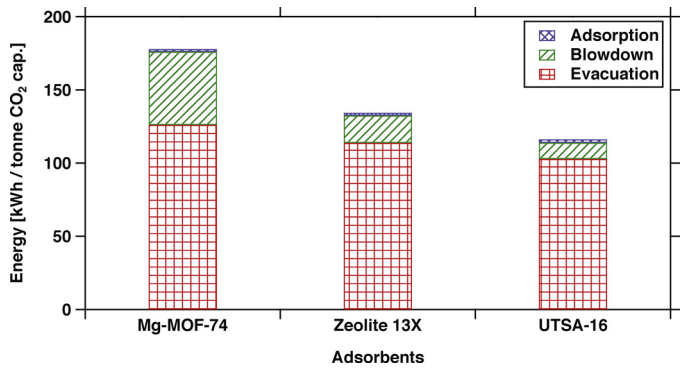

Fig. 8. Energy contribution from constitutive steps corresponding to the minimum energy consumption for Mg-MOF-74, Zeolite 13X and UTSA-16 for the following operating conditions: Mg-MOF-74 – t_{ADS} =90.11 s, t_{BLO} =158.78 s, t_{EVAC} =129.13 s, P_{INT}=0.088 bar, P_L=0.031 bar, v_0 =0.37 m s^{-1}; Zeolite 13X – t_{ADS}=88.05 s, t_{BLO}=164.22 s, t_{EVAC}=66.69 s, P_{INT}=0.138 bar, P_L=0.033 bar, v_0 =0.42 m s^{-1}; UTSA-16 – t_{ADS} =69.39 s, t_{BLO} =69.64 s, t_{EVAC} =61.23 s, P_{INT}=0.181 bar, P_L=0.033 bar, v_0 =0.53 m s^{-1}.

intermediate pressure (P_{INT}) and low pressure (P_L) corresponding to the energy-productivity Pareto curves are plotted. In order to meet the recovery targets, P_L corresponding to the Pareto points for all the three materials converge close to the lower bound for P_L, i.e., 0.03 bar. The achievable purity for a given material depends on the intermediate pressure, P_{INT}. In order to remove the N_2 from the column to achieve high CO_2 purity from the evacuation step, lower P_{INT} is desired. However, lowering P_{INT} also has the tendency to lower CO_2 recovery as it can be lost in the blowdown step. Hence, a desirable material is one where sufficient N_2 can be removed at a higher P_{INT}, and CO_2 can be extracted at a high purity. Among the three materials studied here, nitrogen had the strongest affinity on Mg-MOF-74 and the weakest affinity on UTSA-16. Owing to this, the required P_{INT} for Mg-MOF-74 was $\approx$ 0.06–0.09 bar, compared to $\approx$ 0.16–0.18 bar for UTSA-16, while the Zeolite 13X had P_{INT} intermediate to other two materials as shown in Fig. 7.

The energy contribution of the constitutive steps corresponding to the minimum energy consumption for the three adsorbents is shown in Fig. 8. The energy required by the adsorption and evacuation steps are comparable between the three materials and the key difference arises from the blowdown step. The energy contribution from the blowdown step for Mg-MOF-74 was 50.02 kWh/tonne CO_2 cap. (28.12% of total energy consumption), while for UTSA-16 it was 11.04 kWh/tonne CO_2 cap. (9.49% of total energy consumption). This is directly related to the P_{INT} at the end of the blowdown step shown in Fig. 7. The lower values of P_{INT} for Mg-MOF-74 when compared to the other two adsorbents led to a higher energy consumption in the blowdown step, which was decisive in the total energy consumption for a given adsorbent. It is clear from the above discussions that UTSA-16 was able to achieve the desired purity–recovery targets with the least energy consumption for the 4-step cycle with LPP. The N_2 affinity plays a key role in determining the achievable purity–recovery and thus the energy consumption for the given process.

5. Concluding remarks

The main objective of this work was to evaluate the capability of adsorbent metrics to screen potential adsorbents. Their efficacy was evaluated by performing rigorous process optimisation for four different adsorbents for post-combustion CO_2 capture from dry flue gas. The study indicated that all adsorbent metrics were able to identify the adsorbent that eventually performed poorly. However among the other three, the relative ranking provided by various metrics were very different. After comparing the results of

the process optimisation, only two metrics namely, pure component selectivity and Yang's FOM seemed to provide the ranking, i.e., order of performance. However the difference in magnitudes of these metrics between different materials did not correlate with their process performance.

The optimisation of purity–recovery and energy-productivity provides key insights about the impact of N_2 adsorption on the process performance. For most CO_2 capture materials, increase in CO_2 affinity does not show an improvement in achievable performance. This observation stems from the fact that process constraints such as the lowest practically achievable vacuum pressures (≈ 0.03 bar) do not allow the exploitation of sharper CO_2 isotherms. However the ability of an adsorbent to reject N_2 plays a far more important role than what is usually considered during sorbent selection. This observation, which is now obtained from detailed process optimisation is consistent with the other observations in literature.

We also acknowledge that the process configuration is fixed in this study. It is possible that each adsorbent should be "married" to a process that maximises the potential (Sircar, 2002). This would require more complex approaches such as the use of superstructures (Agarwal et al., 2010). This should be certainly explored in the future. It is also important to stress that eventual success of an adsorbent depends on many other factors that have not been accounted for, e.g. long-term stability, behaviour towards impurities, cost, etc., However, it is our opinion that these considerations are made only if the adsorbent can perform the basic separation task that it is chosen for and methods discussed here allow the researchers to make objective evaluations. In conclusion, this study suggests that including process optimisation tools early in the adsorbent development workflow can in fact be beneficial and that adsorption metrics should be used with caution.

Acknowledgments

Appendix A. Supplementary data

Supplementary data associated with this article can be found, in the online version, at doi:10.1016/j.ijggc.2015.12.033.

References

Aaron, D., Tsouris, C., 2005. Separation of CO_2 from flue gas: a review. Sep. Sci. Technol. 40 (1–3), 321–348.

Abanades, J., Arias, B., Lyngfelt, A., Mattisson, T., Wiley, D., Li, H., Ho, M., Mangano, E., Brandani, S., 2015. Emerging CO_2 capture systems. Int. J. Greenh. Gas Control.

Ackley, M., Stewart, A., Henzler, G., Leavitt, F., Notaro, F., Kane, M., 2000 Feb. 22. PSA apparatus and process using adsorbent mixtures. US Patent 6,027,548.

Agarwal, A., Biegler, L.T., Zitney, S.E., 2010. A superstructure-based optimal synthesis of PSA cycles for post-combustion CO_2 capture. AIChE J. 56 (7), 1813–1828.

Britt, D., Furukawa, H., Wang, B., Glover, T.G., Yaghi, O.M., 2009. Highly efficient separation of carbon dioxide by a metal-organic framework replete with open metal sites. Proc. Natl. Acad. Sci. U. S. A. 106 (49), 20637–20640.

Deb, K., Pratap, A., Agarwal, S., Meyarivan, T., 2002. A fast and elitist multiobjective genetic algorithm: NSGA-II. IEEE Trans. Evol. Comput. 6 (April (2)), 182–197.

Demessence, A., D' Alessandro, D.M., Foo, M.L., Long, J.R., 2009. Strong CO_2 binding in a water-stable, triazolate-bridged metal-organic framework functionalized with ethylenediamine. J. Am. Chem. Soc. 131 (25), 8784–8786.

Ebner, A.D., Ritter, J.A., 2009. State-of-the-art adsorption and membrane separation processes for carbon dioxide production from carbon dioxide emitting industries. Sep. Sci. Technol. 44 (6), 1273–1421.

Finsy, V., Ma, L., Alaerts, L., De Vos, D., Baron, G., Denayer, J., 2009. Separation of CO_2/CH_4 mixtures with the mil-53 (al) metal-organic framework. Microporous Mesoporous Mater. 120 (3), 221–227.

Haghpanah, R., Majumder, A., Nilam, R., Rajendran, A., Farooq, S., Karimi, I.A., Amanullah, M., 2013a. Multiobjective optimization of a four-step adsorption process for postcombustion CO_2 capture via finite volume simulation. Ind. Eng. Chem. Res. 52 (11), 4249–4265.

Haghpanah, R., Nilam, R., Rajendran, A., Farooq, S., Karimi, I.A., 2013b. Cycle synthesis and optimization of a VSA process for postcombustion CO_2 capture. AIChE J. 59 (12), 4735–4748.

Harlick, P.J., Tezel, F.H., 2004. An experimental adsorbent screening study for CO_2 removal from N_2. Microporous Mesoporous Mater. 76 (13), 71–79.

Hu, X., Brandani, S., Benin, A.I., Willis, R.R., 2015. Development of a semiautomated zero length column technique for carbon capture applications: rapid capacity ranking of novel adsorbents. Ind. Eng. Chem. Res. 54 (21), 5777–5783.

Hu, X., Mangano, E., Friedrich, D., Ahn, H., Brandani, S., 2014. Diffusion mechanism of CO_2 in 13x zeolite beads. Adsorption 20 (1), 121–135.

Knaebel, K.S., 1995. For your next separation consider adsorption. Chem. Eng. (N. Y.) 102 (11), 92, 11.

Krishnamurthy, S., Rao, V.R., Guntuka, S., Sharratt, P., Haghpanah, R., Rajendran, A., Amanullah, M., Karimi, I.A., Farooq, S., 2014. CO_2 capture from dry flue gas by vacuum swing adsorption: a pilot plant study. AIChE J. 60 (5), 1830–1842.

LeVeque, R.J., 2002. Finite Volume Methods for Hyperbolic Problems. Cambridge University Press.

Lin, L.-C., Berger, A.H., Martin, R.L., Kim, J., Swisher, J.A., Jariwala, K., Rycroft, C.H., Bhown, A.S., Deem, M.W., Haranczyk, M., Smit, B., 2012 Jul. In silico screening of carbon-capture materials. Nat. Mater. 11 (7), 633–641.

Maring, B.J., Webley, P.A., 2013. A new simplified pressure/vacuum swing adsorption model for rapid adsorbent screening for CO_2 capture applications. Int. J. Greenh. Gas Control 15, 16–31.

Notaro, F., Mullhaupt, J., Leavitt, F., Ackley, M., 1998 Sep. 22. Adsorption process and system using multilayer adsorbent beds. US Patent 5,810,909.

Radosz, M., Hu, X., Krutkramelis, K., Shen, Y., 2008. Flue-gas carbon capture on carbonaceous sorbents: toward a low-cost multifunctional carbon filter for "green" energy producers. Ind. Eng. Chem. Res. 47 (10), 3783–3794.

Rajagopalan, A.K., 2015 August. Material Selection and Process Design for Adsorptive CO_2 Capture. Master's thesis. University of Alberta.

Rege, S.U., Yang, R.T., 2001. A simple parameter for selecting an adsorbent for gas separation by pressure swing adsorption. Sep. Sci. Technol. 36 (15), 3355–3365.

Ruthven, D.M., 1984. Principles of Adsorption and Adsorption Processes. Wiley, New York.

Schumann, K., Unger, B., Brandt, A., Scheffler, F., 2012. Investigation on the pore structure of binderless zeolite 13× shapes. Microporous Mesoporous Mater. 154, 119–123.

Silva, J.A., Schumann, K., Rodrigues, A.E., 2012. Sorption and kinetics of CO_2 and CH_4 in binderless beads of 13x zeolite. Microporous Mesoporous Mater. 158, 219–228.

Sircar, S., 2002. Pressure swing adsorption. Ind. Eng. Chem. Res. 41 (6), 1389–1392.

Susarla, N., Haghpanah, R., Karimi, I., Farooq, S., Rajendran, A., Tan, L.S.C., Lim, J.S.T., 2015. Energy and cost estimates for capturing CO_2 from a dry flue gas using pressure/vacuum swing adsorption. Chem. Eng. Res. Des. 102, 354–367.

van Leer, B., 1979. Towards the ultimate conservative difference scheme. v. A second-order sequel to Godunov's method. J. Comput. Phys. 32 (1), 101–136.

Wiersum, A.D., Chang, J.-S., Serre, C., Llewellyn, P.L., 2013. An adsorbent performance indicator as a first step evaluation of novel sorbents for gas separations: application to metal organic frameworks. Langmuir 29 (10), 3301–3309.

Xiang, S., He, Y., Zhang, Z., Wu, H., Zhou, W., Krishna, R., Chen, B., 2012 July. Microporous metal-organic framework with potential for carbon dioxide capture at ambient conditions. Nat. Commun. 3, 954.

Xiao, P., Zhang, J., Webley, P., Li, G., Singh, R., Todd, R., 2008. Capture of CO_2 from flue gas streams with Zeolite 13X by vacuum-pressure swing adsorption. Adsorption 14 (4–5), 575–582.

Xu, D., Zhang, J., Li, G., Xiao, P., Webley, P., Zhai, Y.-C., 2011. Effect of water vapor from power station flue gas on CO_2 capture by vacuum swing adsorption with activated carbon. J. Fuel Chem. Technol. 39 (3), 169–174.

Yang, R., 1997. Gas Separation by Adsorption Processes. Chemical Engineering. Imperial College Press.

Yazaydin, A.O., Snurr, R.Q., Park, T.-H., Koh, K., Liu, J., LeVan, M.D., Benin, A.I., Jakubczak, P., Lanuza, M., Galloway, D.B., Low, J.J., Willis, R.R., 2009. Screening of metal-organic frameworks for carbon dioxide capture from flue gas using a combined experimental and modeling approach. J. Am. Chem. Soc. 131 (51), 18198–18199.

Zhang, J., Webley, P.A., 2008. Cycle development and design for CO_2 capture from flue gas by vacuum swing adsorption. Environ. Sci. Technol. 42 (2), 563–569.

Zhang, Z., Yao, Z.-Z., Xiang, S., Chen, B., 2014. Perspective of microporous metal-organic frameworks for CO_2 capture and separation. Energy Environ. Sci. 7, 2868–2899.